Improving Hydro-formability of a Ferritic Stainless Steel Tube Through Severe Plastic Deformation

M.H. FARSHIDI, Y. KITANO, M. YUASA, and H. MIYAMOTO

The aim of this work is to improve the hydro-formability of a 409L ferritic stainless tube through a treatment involving severe plastic deformation followed by annealing. For this purpose, the variation in hydro-formability is determined in terms of parameters like the circumferential *R*-value and the circumferential elongation after application of the abovementioned treatment. In addition, the deformation-induced surface roughening of the tube, called ridging, is measured through tension tests before and after the treatment. Moreover, the evolution in tube texture caused by the treatment is studied to reveal the relationship between the hydro-formability parameters and the texture. The results show that the treatment dramatically improves the hydro-formability through a marked modification in texture. For example, the emergence of the $\{110\}\langle 100\rangle$ texture component through the present treatment causes a noticeable increase in the circumferential elongation and the circumferential *R*-value of the tube while decreasing the degree of ridging.

https://doi.org/10.1007/s11661-018-4917-4

I. INTRODUCTION

FERRITIC stainless steels (FSSs) typically ensure a higher resistance to stress corrosion cracking as well as lower prices in comparison to austenitic stainless steels. Thus, they are promising candidates for corrosive environments, especially those containing the chlorides ion.[1,2] However, the formability of these steels is lower than that of their austenitic counterparts.[3–5] For instance, FSSs usually suffer from surface roughening during tensile forming processes like deep-drawing and hydro-forming. This type of defect, often called ridging, has mainly been attributed to the appearance of a specific texture during the casting and hot-rolling of FSSs. More specifically, it has been reported that the $\langle 100\rangle$ orientations of the large columnar grains of an FSS slab are parallel to the slab's normal direction, owing to the directional solidification that occurs during slab casting. This solidification texture fiber is complemented by two other relatively strong texture fibers during the subsequent hot-rolling process in which the $\{111\}$ planes of the grains are almost identical to the rolling plane and/or the $\langle 110\rangle$ orientations of the grains are almost parallel to the rolling direction. These special hot-rolling texture fibers are usually called γ-fiber and α-fiber, respectively. Since grains oriented on the texture fibers formed during the casting and rolling of FSSs show different Schmid factors, their slip behaviors tend to differ, and therefore, they induce ridging during subsequent tensile forming processes.[4–7] The other reason for the poor formability of FSSs is their small *R*-value. The average *R*-value of FSS sheets is typically reported to be between 1.0 and 1.5 depending on the processing conditions. However, the exact *R*-value is dependent on the direction of tensile forming. For example, the *R*-value can be as low as 0.5 for one specific direction of a rolled FSS sheet.[7–10] The differences in *R*-value are mainly related to the appearance of the specific texture fibers mentioned above. For instance, the *R*-values of the different directions of a sheet oriented exactly on the $\{111\}\langle 110\rangle$ texture component are found to be between 1.5 and 2.2 by using a crystal plasticity finite element (CPFE) simulation. The corresponding values for a sheet oriented exactly on the $\{100\}\langle 110\rangle$ texture component are found to be between 0.1 and 0.9.[10,11] Thus, it can be inferred that modification of the texture of an FSS is key to obtaining a favorable formability.

Modification of the conventional texture that appeared during casting and rolling of an FSS is difficult since it does not undergo the austenite-to-ferrite allotropic transformation required for grain refinement. In addition, the restoration of an FSS during annealing usually occurs by recovery, rather than recrystallization. This hinders the texture modification of FSS because it

M.H. FARSHIDI is with the Department of Materials Science and Metallurgical Engineering, Ferdowsi University of Mashhad, Azadi Square, Mashhad, Iran. Contact e-mail: farshidi@um.ac.ir Y. KITANO, M. YUASA, and H. MIYAMOTO are with the Department of Mechanical Engineering, Doshisha University, Kyotanabe city, Kyoto, Japan.
Manuscript submitted March 12, 2018.

Published online: 25 September 2018

reduces the grain refinement capability.[4–7] Thus, numerous studies have paid attention to the texture modification of FSSs. A number of these studies attempted to induce shear bands through a pre-forming process that can promote nucleation of recrystallization during the subsequent annealing, and succeeded in modifying the texture that appeared as a result of annealing.[7,8] Decreasing the slab-forming temperature and processing by severe plastic deformation (SPD) are two approaches that have been proposed to induce shear bands in FSSs.[4,7,8]

Processing of an alloy by SPD is advantageous because it causes grain refinement of the alloy and modification of its texture. Note that the term "SPD process" refers to a compressive deformation process in which considerable strain is imposed on the specimen without a significant change in its dimensions.[12] Although various studies have focused on the SPD processing of alloys during the past few decades, most of these studies have considered the SPD processing of copper alloys and aluminum alloys while SPD processing of FSSs has remained largely neglected.[12,13] On the other hand, SPD processing of tubes has recently received increasing attention, owing to their widespread industrial applications. Different processes have been developed for this purpose, such as tube channel pressing (TCP), accumulative spin bonding, and high-pressure tube twisting.[14–16] However, most previous work on this topic has focused on the grain refinement of tubes, while the effect of SPD processing on the texture modification of tubes has been largely ignored.

The aim of the present study is to improve the hydro-formability of a 409L FSS tube through the recently developed TCP process. For this purpose, tubular FSS specimens are treated by different passes of TCP followed by post-annealing, after which the changes in their hydro-formability are determined through tension tests. In addition, the evolution in their microstructure and texture is studied using optical microscopy (OM), electron back-scattering diffraction (EBSD), and X-ray diffraction (XRD). These studies led to an understanding of the relationship between the hydro-formability of a treated tube and its microstructure/texture.

II. PROCESS, MATERIALS, AND EXPERIMENTS

Among abovementioned SPD processes of tube, TCP is more practically applicable due to its little need to complicated machinery devices as well as its ability to process tubes manufactured in different sizes.[17–19] Therefore, TCP could be nominated as an industrial SPD process. A prospective application of TCP could be arisen in manufacturing of superconducting cavities where controlling of texture of niobium tube is important. Figure 1(a) illustrates the principles of the TCP process. As can be seen, the tube is passed through a bottleneck-shaped channel during TCP processing, which induces hoop strains and shear strains in the tube wall. The diameter and thickness of the FSS tube used are 42.7 mm and 1 mm, respectively. Figure 1(b) illustrates the manufactured TCP die and tubular FSS specimens. To decrease the heterogeneity of the plastic strain imposed by TCP, the die is manufactured according to the new geometry of TCP process. The die curvature radius (R), channel angle ($\theta_{channel}$), and die convex height (Δr_{die}) are set to 2 mm, 150 deg, and 1 mm, respectively. Other die design parameters are related to these parameters, as shown in previous works.[17–19] Figure 1(c) shows the results of an FEM simulation for the distribution of the plastic strain imposed on an FSS tube through TCP processing using the mentioned die. As can be seen, the average plastic strain induced by one TCP pass is about 0.85. In addition, there is heterogeneity in distribution of strain after imposition of one pass of TCP which reported to remain almost constant during imposition of more TCP passes.[20] More details about the process, the effect of the die geometrical parameters/tube dimensions on the strain distributions and the FEM simulation method have been presented elsewhere.[17–19]

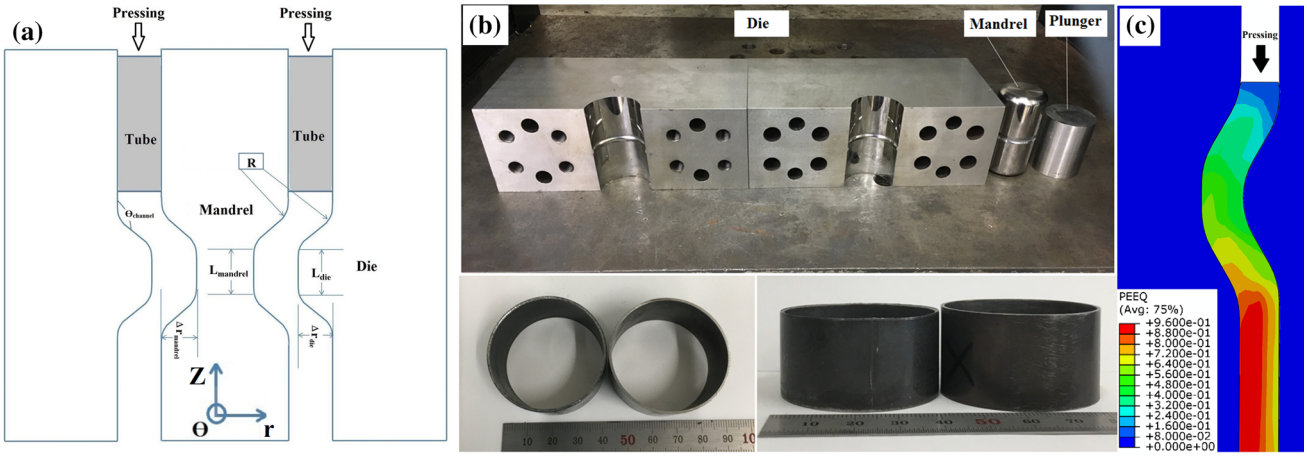

Fig. 1—(*a*) Schematic of TCP process, (*b*) the manufactured TCP die and tubular FSS 409L specimens, and (*c*) distribution of imposed plastic strain through one TCP pass using the manufactured die.

The typical alloying elements of 409L FSS are 11 pct Cr, 1 pct Mn, and 1 pct Si, while the concentrations of C and N are less than 0.03 pct. The 409L FSS tube is received in welded form. It was fabricated by electric resistance welding of a rolled sheet. The longitudinal direction (LD), circumferential direction (CD), and outward direction (OD) of the tube are, respectively, identical to the rolling direction (RD), transverse direction (TD), and normal direction (ND) of the sheet. The as-received tube is cut into 25-mm-long specimens and then subjected to 0, 1, 2, and 3 passes of TCP processing at 423 K using a loading rate of 1 mm/s. For reduction of friction effect, surfaces of die, mandrel, and specimen are smeared by MoS_2 lubricant before initiation of the process. Afterwards, the specimen is inserted into TCP die set and after imposition of each TCP pass, the die set containing the specimen is rotated for 180 deg and the next pass is imposed from the opposite side. After imposition of projected TCP passes, the die set is opened and the specimen is expelled out using a thinner mandrel. The time between successive TCP passes is about 15 min and specimens are subjected to a 3-min anneal at different temperatures, as shown in Table I. Hereafter, xTCP will refer to a specimen subjected to × TCP passes before annealing, and xTCPA will refer to a specimen treated by × TCP passes followed by annealing. Since the tube's circumferential properties govern its hydro-formability, hoop tension tests are performed on TCPA specimens to determine their elongations and their *R*-values along the circumferential direction of the tube. Also, tension tests are conducted along the longitudinal direction of TCPA specimen up to a plastic strain of 15 pct to determine the extent of ridging on the specimens' surfaces through surface roughness measurements by laser microscopy.

To characterize the microstructure and texture of the specimens, OM and EBSD samples are obtained from the plane normal to the CD of the tube. In addition, XRD samples are obtained from the plane normal to the tube's OD and prepared by unbending. Figure 2 shows tube surfaces examined by OM, EBSD, and XRD. OM samples are mechanically polished and etched with a solution consisting of equal weights of nitric acid, hydrochloric acid, and glycerin. EBSD samples are prepared by mechanical polishing and studied using a JEOL JSM-7001F scanning electron microscope, and the software Inca 4.09 is used to interpret the EBSD results. The interactive texture module of Inca 4.09 is used to determine volume of different texture components as a fraction of their volume in a completely random distribution.

Table I. The Annealing Temperatures Used for Different Specimens

Imposed TCP Pass Number	0	1	2	3
Annealing temperature (°K)	1023	1073	1123	1173

III. RESULTS AND DISCUSSION

Figure 3 compares the microstructures of TCP-processed specimens before and after annealing. As can be seen in Figures 3(a) through (c), the microstructures of TCP-processed specimens before annealing are characterized by elongated grains and in-grain micro shear bands (MSBs). For more explanation, an MSB is assumed to be a micron-sized shear band extending inside a grain, formed as a result of local plastic instability. It is generally believed that MSBs are formed as a result of the increase in the misorientations of aligned sub-boundaries inside a grain due to the increase in imposed plastic strain.[21,22] As can be seen in Figures 3(a) through (c), MSBs are induced along different directions of TCP-processed specimens. This can be attributed to the imposition of multi-directional strains through TCP processing, as discussed in the literature.[23] In addition, the density of MSBs increases with increasing number of TCP passes. As shown in Figures 3(d) through (f), equiaxed grains are typical of the microstructures of TCPA-treated specimens. Moreover, 2TCPA and 3TCPA grains are generally characterized by sharp, well-adjusted boundaries, while 1TCPA grains are often defined by bowed and unadjusted boundaries. These microstructures suggest that during annealing, 2TCPA and 3TCPA specimens are almost completely recrystallized while 1TCPA is only partially recrystallized.[24]

Figure 4 compares the results of hoop tension tests for TCPA-treated specimens. As shown in Figure 4(a), the strength and the elongation of tube increase markedly as a result of the treatment. The increase in strength can hardly be related to work hardening during TCP processing, since the specimens are clearly

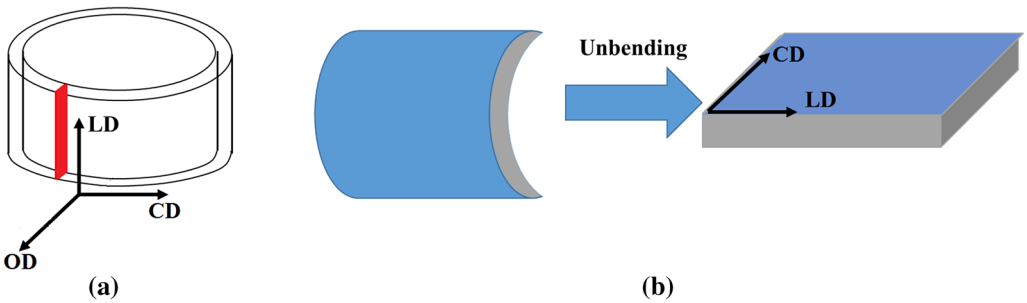

Fig. 2—Schematics of tube surfaces observed by (*a*) OM and EBSD and (*b*) XRD.

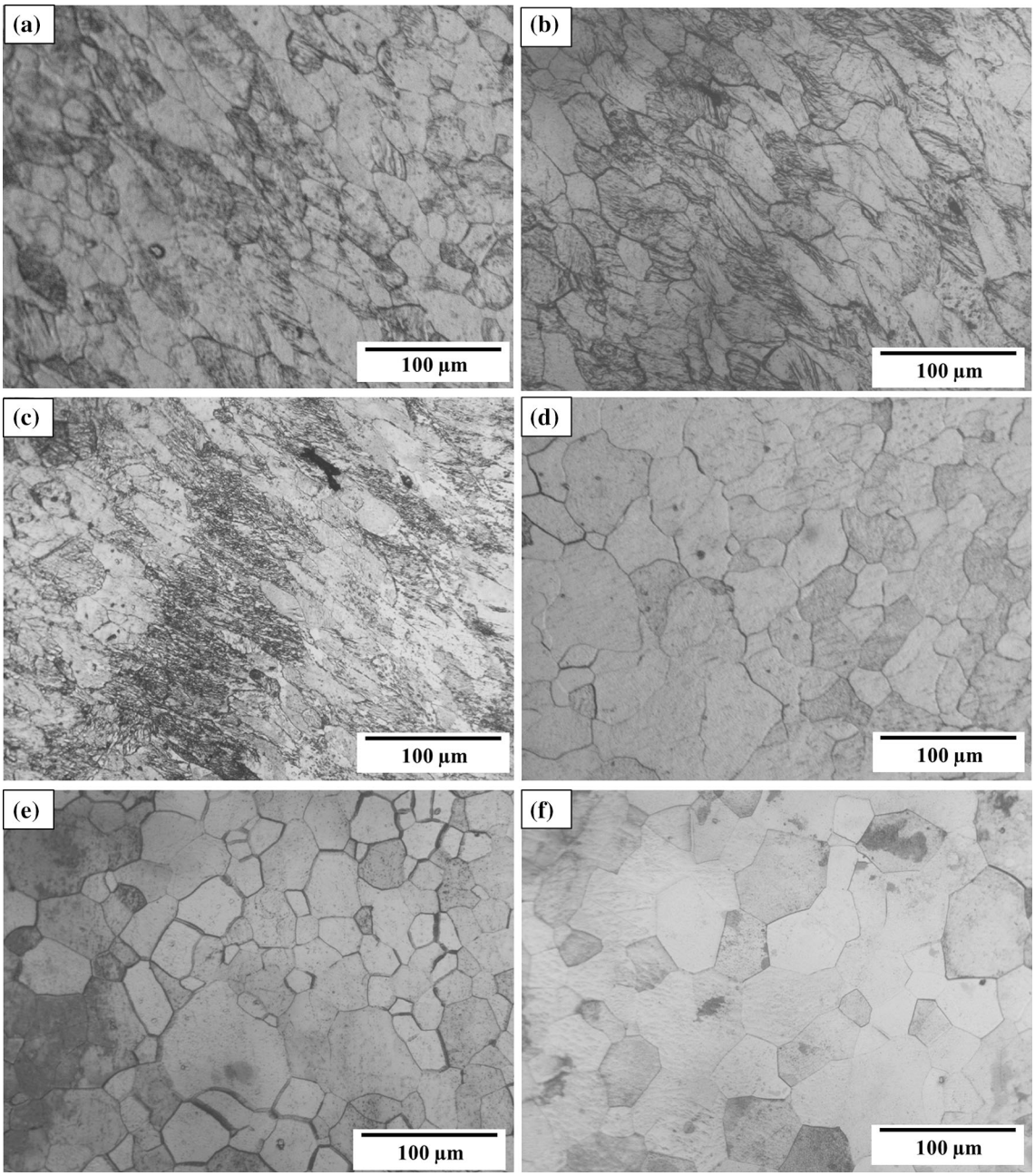

Fig. 3—Microstructures of TCP-processed specimens before and after annealing: (*a*) 1TCP, (*b*) 2TCP, (*c*) 3TCP, (*d*) 1TCPA, (*e*) 2TCPA, and (*f*) 3TCPA.

recrystallized during the subsequent annealing. In addition, prior work hardening should decrease the elongation of TCPA-treated specimens, despite the evidence in Figure 4(a). Therefore, the simultaneous increase in the elongation and strength of the tube through TCPA processing could be correlated with the evolution of its texture. Figure 4(b) plots the variation of the circumferential *R*-value of the tube due to the TCPA treatment. As can be seen, the circumferential *R*-value of the 0TCPA specimen is about 0.9, which is reasonably low for the hydro-forming process. The circumferential *R*-values of other TCPA-treated specimens are significantly larger, which demonstrates the improvement in the circumferential *R*-value of the tube through the present treatment. Figure 5(a) shows the surfaces of LD tension samples after imposing a strain of 15 pct. As can be seen, the extent of ridging on the surfaces of these samples decreases with increasing number of TCP passes. Figures 5(b) through (e) show the measured surface roughness of the samples in Figure 5(a). As shown here, the surface roughness decreases with increasing number of TCP passes, which confirms the decrease in ridging. Considering explanations of Figures 4 and 5, it can be inferred that the tube texture is modified dramatically by the TCPA treatment.

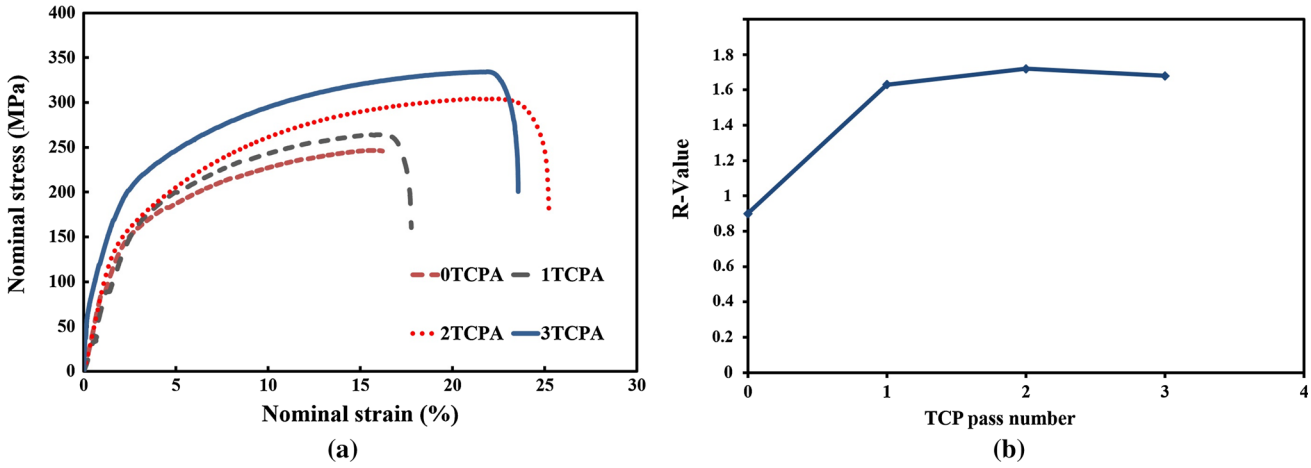

Fig. 4—(*a*) Circumferential stress-strain curves of TCPA-treated specimens; (*b*) variation of circumferential *R*-value of tube induced by TCPA treatment.

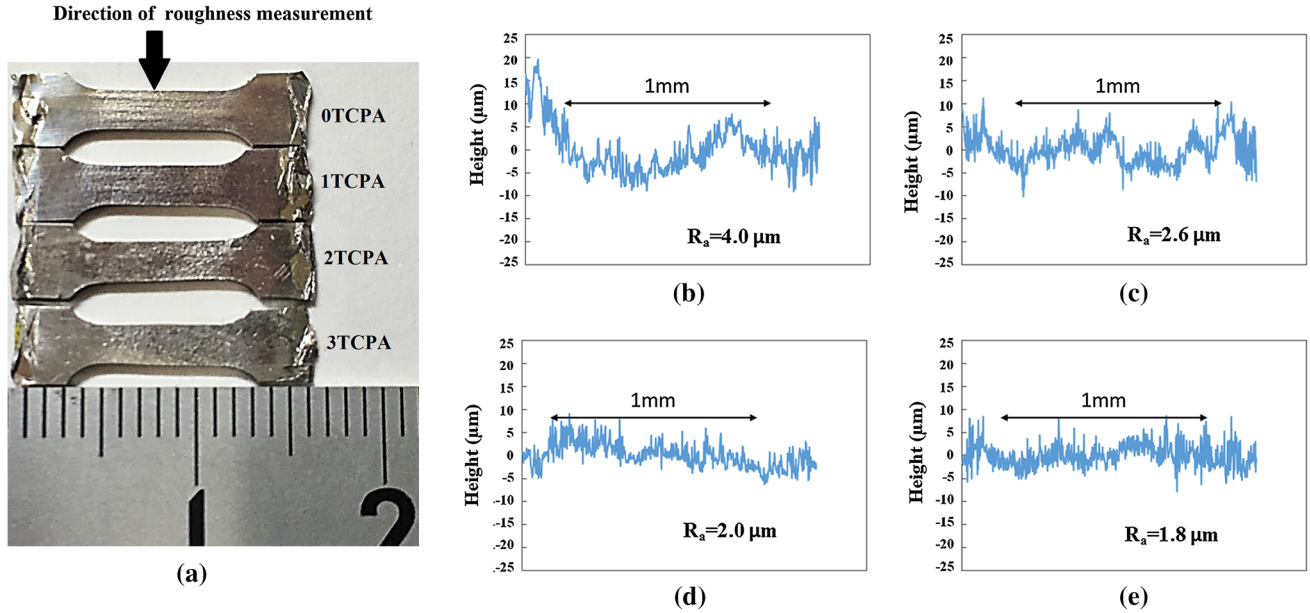

Fig. 5—(*a*) Surfaces of TCPA-treated samples after the LD tension test. Measured surface roughness of samples shown in (a): (*b*) 0TCPA, (*c*) 1TCPA, (*d*) 2TCPA, and (*e*) 3TCPA.

Figure 6 compares the XRD results for TCPA-treated specimens. As shown here, grains with {100} and {111} planes normal to the OD display high intensities inside the 0TCPA specimen. As mentioned above, these texture fibers develop during casting and hot-rolling of the sheet used for tube fabrication and often cause ridging during the subsequent tensile forming. As can be seen in Figures 6(a) and (b), the intensities of the grains with {100} and {111} planes normal to the OD decrease with increasing number of TCP passes. By contrast, the intensities of grains with the {110} planes normal to the OD increases with increasing number of TCP passes, as shown in Figure 6(c). These results indicate the appearance of a new texture during TCPA treatment, as will be discussed later.

Figure 7 shows orientation image maps of TCPA-treated specimens. The ⟨100⟩, ⟨110⟩, and ⟨111⟩ orientations of the grains are indicated by red, green and blue, respectively. As shown in Figure 7(a), the {111} and {100} planes of the grains normal to the OD of the 0TCPA specimen have high intensities. In addition, high intensity of grains with ⟨110⟩ orientations parallel to the LD can be observed inside the 0TCPA specimen. The presence of such strong texture fibers indicates the existence of a conventional casting and rolling texture inside the 0TCPA specimen. As shown in Figures 7(a) through (d), TCPA treatment increases the intensity of the grains' {110} planes normal to the OD, which is in exact agreement with the XRD results. Furthermore, TCPA treatment dramatically increases the intensity of

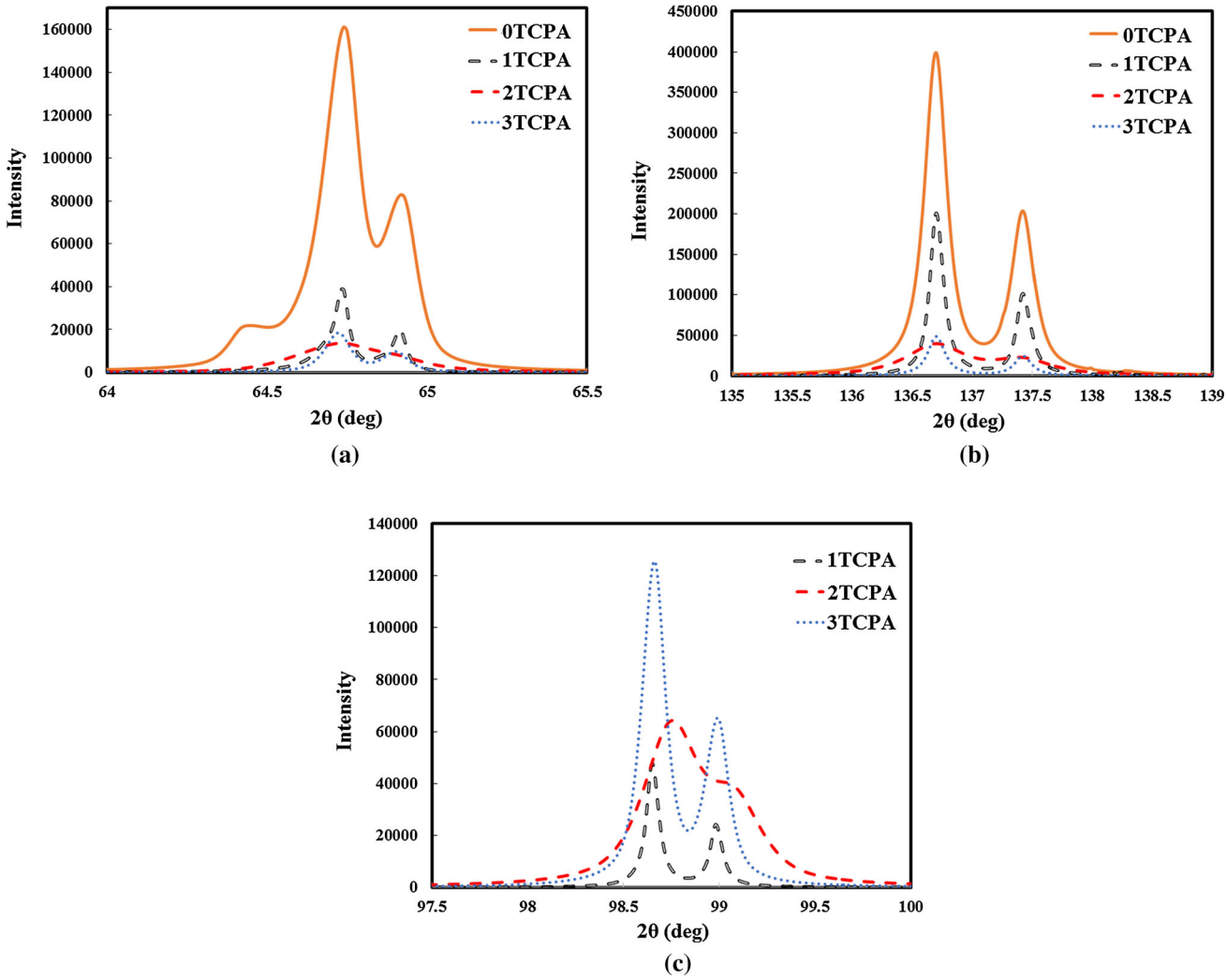

Fig. 6—XRD results showing the intensities of grains with (*a*) {100} planes, (*b*) {111} planes, and (*c*) {110} planes normal to OD.

the grains with ⟨100⟩ orientations parallel to LD. These results indicate that the applied treatment alters the typical casting and rolling texture of FSS through the development of a new texture component whose {110} planes and ⟨100⟩ orientations are normal to the OD and parallel to the LD of the tube, respectively. Table II compares several typical texture components in terms of the results of CPFE simulations for their transversal *R*-values[10,11,25,26] and their relative amounts in TCPA-treated specimens. Note that, the tabulated amounts for the texture components are determined by a tolerance of 15° using the EBSD results. As shown in Table II, TCPA treatment dramatically increases the {110}⟨100⟩ texture component while significantly decreasing the other texture components. This weakens the typically strong rolling and casting texture of FSS. Thus, the decrease in ridging through TCPA treatment can be linked to weakening of the typical texture. In addition, a comparison of the transversal *R*-values presented in Table II reveals that the dramatic increase in the circumferential *R*-value of the tube upon TCPA treatment is due to the emergence of the {110}⟨100⟩ texture component, which shows the highest transversal *R*-value among all the texture components.

Figure 8 shows the TCP-induced micro-textural evolution occurring before annealing. As shown here, the {110}⟨100⟩ texture component appears in different grains as a result of TCP processing due to occurrence of MSBs. Similarly, it has been reported that this texture component, often referred to as Goss, is a deformation texture encountered within shear bands induced by cold deformation.[27–29] Given all of the above, the high intensity of the {110}⟨100⟩ texture component inside the TCPA-treated specimens can be attributed to the appearance of TCP-induced MSBs oriented this texture component, as will be discussed later.

Figure 9 plots the variation in misorientation for xTCP and xTCPA specimens along the double-sided arrows in Figures 7 and 8. As shown in Figures 9(a) through (c), the maximum misorientations along the arrows for the xTCP specimens range from 6 to 18 deg. This is indicative of cold-deformed microstructures and the negligible effect of dynamic restoration phenomena like recovery and recrystallization.[24] Indeed, the

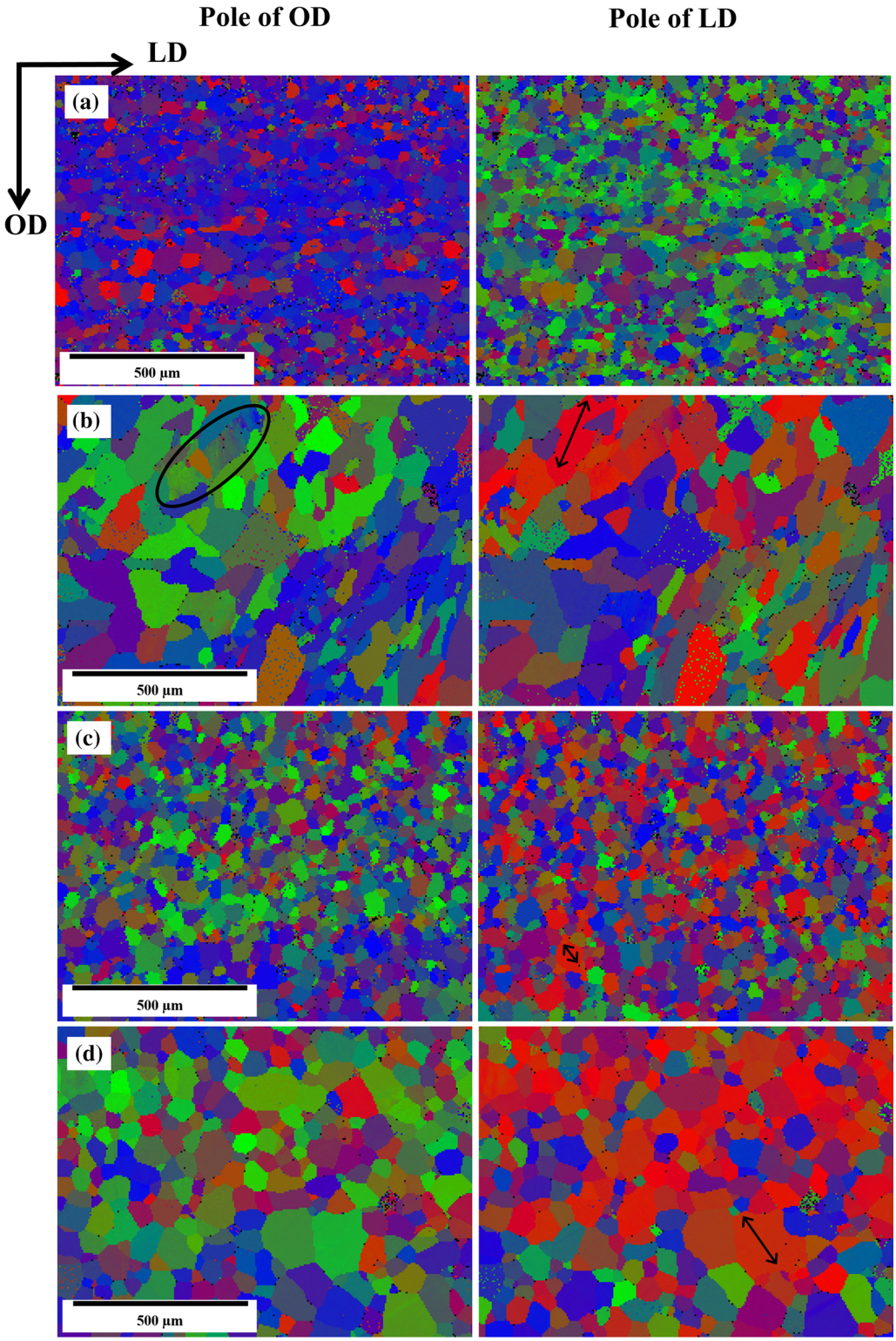

Fig. 7—Orientation image maps of TCPA-treated specimens: (*a*) 0TCPA, (*b*) 1TCPA, (*c*) 2TCPA, and (*d*) 3TCPA. The ellipse in (b) indicates a non-recrystallized region.

dynamic restoration that occurs during TCP processing is most likely negligible, since the deformation temperature is much lower than the restoration temperature of the alloy. By contrast, the maximum misorientations inside the 2TCPA and 3TCPA grains are about 1 deg, while the maximum misorientation in 1TCPA is about 2.5 deg, as shown in Figures 9(d) through (f). Moreover, close examination of the microstructure of the 1TCPA specimen shown in Figure 7(b) reveals at least one non-recrystallized region. These results indicate that the

Table II. Typical FSS Texture Components, Their Transversal *R*-Values[10,11,21,22] and Their Amounts in TCPA-Treated Specimens

Texture Component	{110}⟨100⟩	{211}⟨110⟩	{100}⟨110⟩	{111}⟨112⟩	{111}⟨110⟩
Transversal *R*-value	∞	0.8	0.1	1.4	2.1
Quantity inside 0TCPA	0.4 pct (0.2)	11 pct (2.4)	2 pct (0.9)	28.4 pct (6.3)	9.3 pct (2.1)
Quantity inside 1TCPA	8.7 pct (4.1)	3.3 pct (0.7)	0.7 pct (0.3)	9.6 pct (2.1)	6.9 pct (1.5)
Quantity inside 2TCPA	6.4 pct (3.1)	4 pct (0.9)	0.2 pct (0.1)	12.3 pct (2.7)	4.1 pct (0.4)
Quantity inside 3TCPA	16 pct (7.6)	1.2 pct (0.3)	0 (0)	8.4 pct (1.9)	1.6 pct (0.4)

The figures in parentheses are the amounts of the texture components expressed as a fraction of their relative amounts in a random distribution.

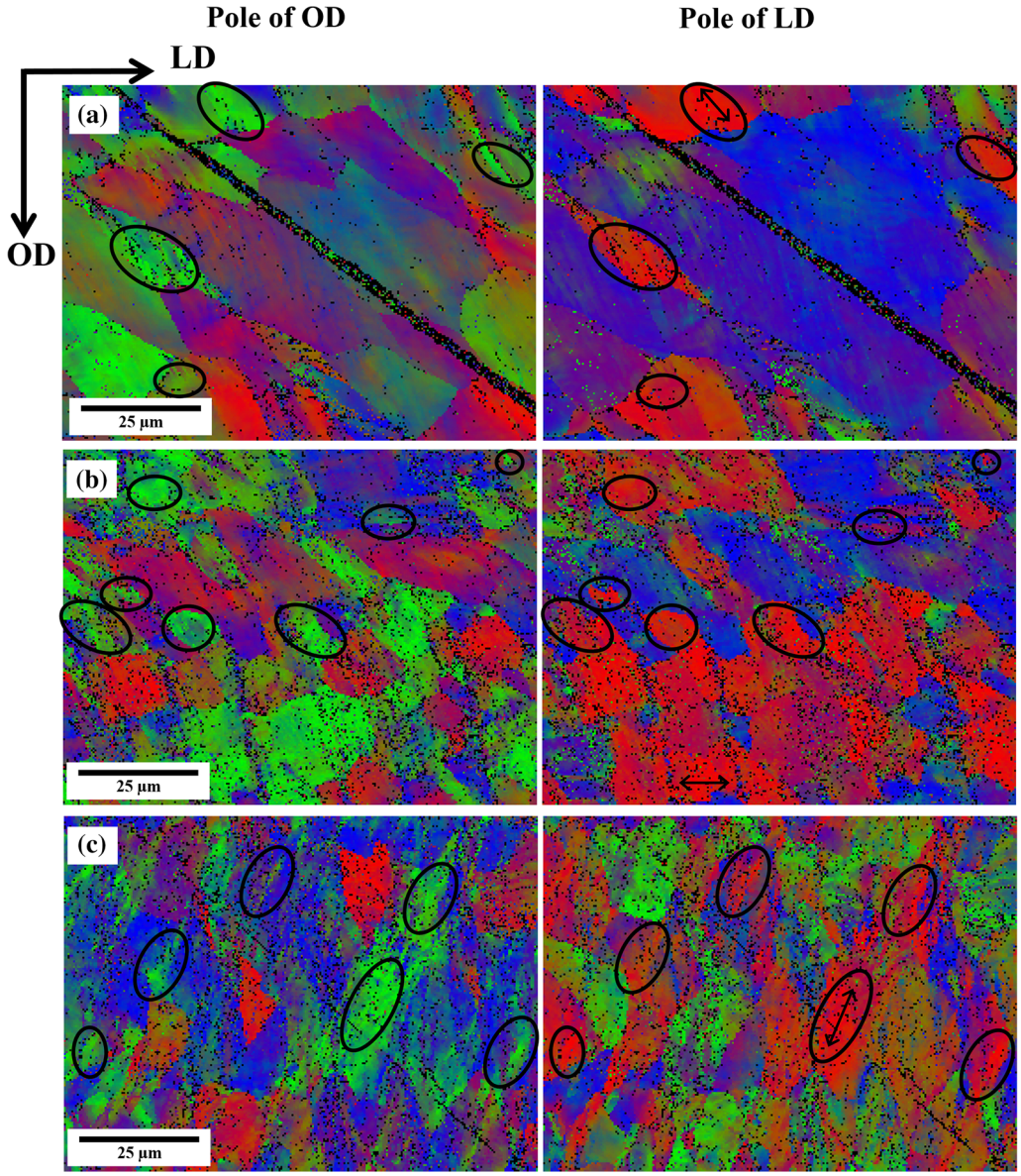

Fig. 8—Micro-texture of TCP-processed specimen before annealing subjected to: (*a*) 1, (*b*) 2, and (*c*) 3 TCP passes. Black ellipses indicate MSBs oriented {110}⟨100⟩ texture component.

recrystallization occurring in 2TCPA and 3TCPA goes to completion while that occurring in 1TCPA is partial.[24]

On the basis of Figures 3 through 9, it can be inferred that TCP processing induces MSBs in the 409L FSS tube. These MSBs can act as nucleation sites for static recrystallization during the subsequent anneal, as shown in previous studies.[21,27,29,30] Note that, nucleation can occur by accelerated recovery in the MSBs at the start of anneal since the stored energy in the MSBs is higher than elsewhere in the grain.[24] Since TCP-induced MSBs

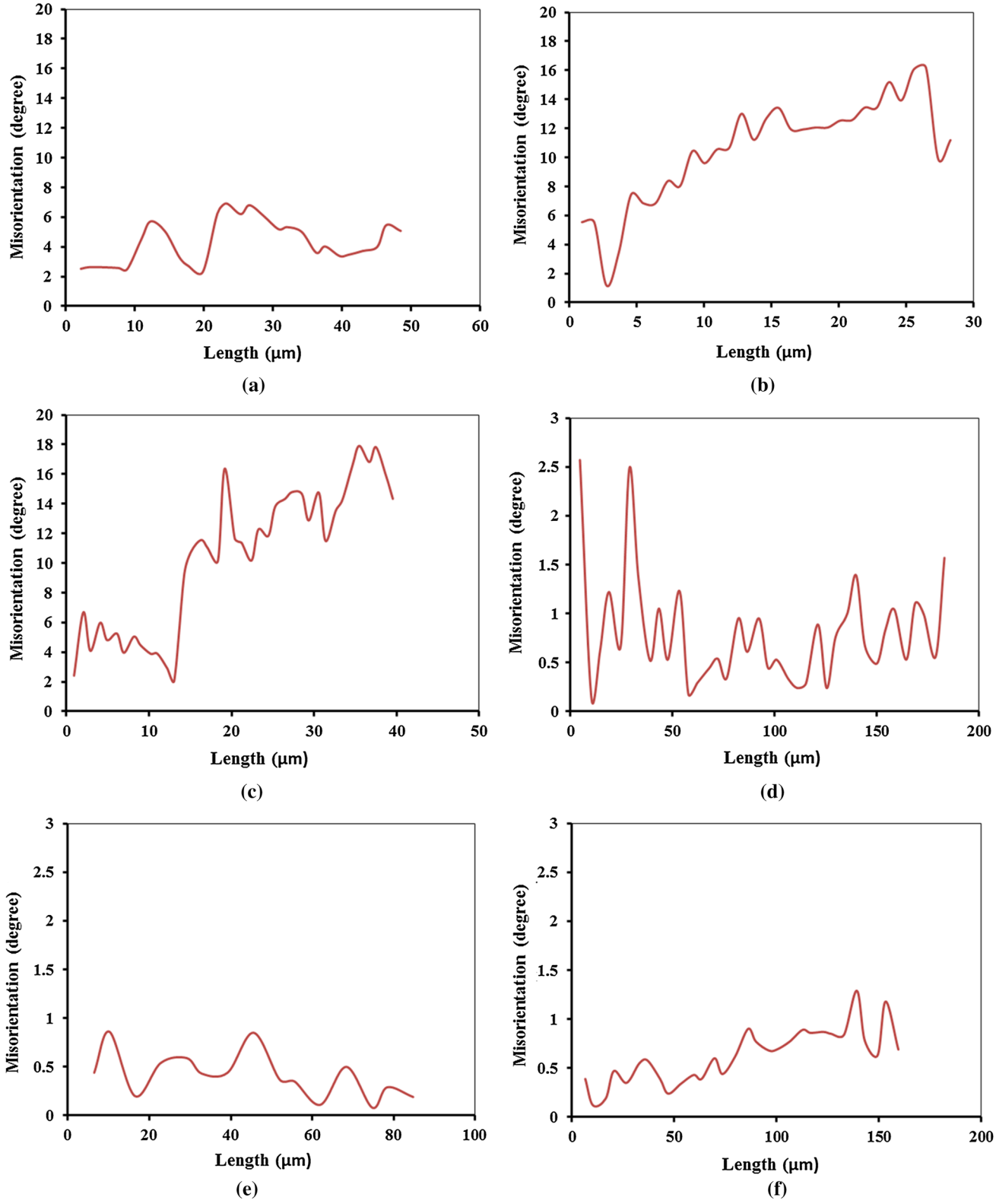

Fig. 9—Variation of misorientation along the double-sided arrows in Figs. 7 and 8: (*a*) 1TCP, (*b*) 2TCP, (*c*) 3TCP, (*d*) 1TCPA, (*e*) 2TCPA, and (*f*) 3TCPA.

are often found in the Goss texture component, a high concentration of this texture component is observed in the TCPA specimen and therefore the typical casting and rolling texture of FSS disappears. Thus, the circumferential *R*-value and the circumferential elongation of the tube increase, while the probability of ridging

decreases as a result of TCPA treatment. However, there are two points that need to be addressed. First, the circumferential elongation of 3TCPA is clearly lower than that of 2TCPA although the amount of Goss texture component in 3TCPA is markedly larger than that in 2TCPA, as shown in Figure 4(a) and Table II. Correspondingly, while the amount of Goss texture component in 1TCPA is significantly greater than that in 0TCPA, the circumferential elongations of 1TCPA and 0TCPA are almost the same. This can be attributed to the impressively finer grain sizes of 0TCPA and 2TCPA, which render them more ductile. For instance, the grain sizes of 0TCPA, 1TCPA, 2TCPA, and 3TCPA are determined to be 35, 78, 36, and 64 μm, respectively, from the EBSD results. These differences in grain size induced by the applied treatment are due to the use of different annealing temperatures and the imposition of different plastic strains. Note that, the number of recrystallization nucleation sites increases with increasing number of TCP passes, which can result in a decreased grain size after recrystallization. On the other hand, the increase in annealing temperature caused by the increased number of TCP passes (see Table I) may lead to grain coarsening usually referred to as secondary recrystallization.[24] These competing effects can explain the appearance of different grain sizes through the applied treatment. Secondly, since the appearance of the Goss texture component is due to the MSBs induced by TCP processing, one would expect the amount of this texture component to increase with increasing number of TCP passes. This is indeed found to be the case (see Table II), with one notable exception: the amount of the Goss texture component in 2TCPA is lower than that in 1TCPA. This can be explained as follows. The $\{110\}\langle 100\rangle$ (Goss) and $\{111\}\langle 112\rangle$ texture components compete during primary recrystallization and therefore the amount of the Goss texture component can decrease during primary recrystallization.[30–32] This is due to the greater boundary energy of the Goss grains, which causes the annihilation of small grains found in this texture component during primary recrystallization. However, since the boundary mobility of Goss grains is considerably larger than that of other grains, the remaining Goss grains show a rapid growth during secondary recrystallization, which leads to a considerable increase in the amount of this texture component.[32–34] Thus, the lower fraction of the Goss texture component in 2TCPA can be accounted for by the completion of primary recrystallization and the negligible secondary recrystallization in this specimen. On the basis of these explanations, one can propose that the hydro-formability of an FSS tube can be optimized through TCP processing followed by a controlled anneal to produce a fine-grained microstructure and the desired texture.

IV. CONCLUSION

An FSS 409L tube is treated by TCP processing followed by annealing to improve its hydro-formability. On the basis of the present results and discussion, the following conclusions are drawn:

(1) TCP processing of the FSS tube induces MSBs throughout its microstructure, which can act as nucleation sites for recrystallization during the subsequent annealing.
(2) TCP-induced MSBs are often found in the Goss texture component, in which the $\{110\}$ plane and $\langle 100\rangle$ orientations are, respectively, normal to the OD and parallel to the LD of the tube. Therefore, the amount of the Goss texture component increases dramatically during the TCPA treatment.
(3) TCPA treatment causes the circumferential elongation and circumferential *R*-value of the tube to increase and the ridging to decrease. This is because of the weakening of the typical casting and rolling texture of FSS associated with the appearance of the Goss texture component. These results point to the enhanced hydro-formability of the TCPA-treated tube.
(4) To optimize the hydro-formability of an FSS tube, the TCP process should be followed by a controlled anneal to produce a fine-grained microstructure and a desired texture.

ACKNOWLEDGMENTS

The authors wish to thank the research board of Doshisha University and Ferdowsi University of Mashhad (FUM) for the financial support and the provision of research facilities used in this work.

REFERENCES

1. C.L. Chen, A. Richter, R. Kögler, M. Griepentrog, and P. Reinstadt: *J. Alloys Compd.*, 2014, vol. 615, pp. S448–53.
2. M. Kaneko and H.S. Isaacs: *Corros. Sci.*, 2002, vol. 44, pp. 1825–34.
3. V. Taylan, R.H. Wagoner, and J.K. Lee: *Metall. Mater. Trans.*, 1998, vol. 29A, pp. 2161–72.
4. H. Miyamoto, T. Xiao, T. Uenoya, and M. Hatano: *ISIJ Int.*, 2010, vol. 50 (11), pp. 1653–59.
5. H.J. Shin, J.K. An, S.H. Park, and D.N. Lee: *Acta Mater.*, 2003, vol. 51, pp. 4693–4706.
6. P.D. Wu, H. Jin, Y. Shi, and D.J. Lloyd: *Mater. Sci. Eng. A*, 2006, vol. 423, pp. 300–05.
7. C. Zhang, Z. Liu, and G. Wang: *J. Mater. Process. Technol.*, 2011, vol. 211 (6), pp. 1051–59.
8. Y. Yazawa, Y. Ozaki, Y. Kato, and O. Furukimi: *JSAE Review*, 2003, vol. 24, pp. 483–88.
9. M.Y. Huh and O. Engler: *Mater. Sci. Eng. A*, 2001, vol. 308, pp. 74–87.
10. K.M. Lee, M.Y. Huh, S. Park, and O. Engler: *ISIJ Int.*, 2012, vol. 52 (3), pp. 522–29.
11. J.I. Hamada, K. Agata, and H. Inoue: *Mater. Trans.*, 2009, vol. 50 (4), pp. 752–58.
12. Y. Estrin and A. Vinogradov: *Acta Mater.*, 2013, vol. 61, pp. 782–817.
13. I. Sabirov, M.Y. Murashkin, and R.Z. Valiev: *Mater. Sci. Eng. A*, 2013, vol. 560, pp. 1–24.
14. M.H. Farshidi and M. Kazeminezhad: *J. Mater. Des. Appl.*, 2016, vol. 230, pp. 263–72.
15. M.S. Mohebbi and A. Akbarzadeh: *Mater. Sci. Eng. A*, 2010, vol. 528, pp. 180–88.
16. M. Arzaghi, J.J. Fundenberger, L.S. Toth, R. Arruffat, L. Faure, B. Beausir, and X. Sauvage: *Acta Mater.*, 2012, vol. 60, pp. 4393–4408.

17. M.H. Farshidi and M. Kazeminezhad: *J. Mater. Eng. Perform.*, 2012, vol. 21, pp. 2099–2105.
18. M.H. Farshidi: *Iran. J. Mater. Form.*, 2016, vol. 3 (2), pp. 64–78.
19. M.H. Farshidi: *Iran. J. Mater. Form.*, 2018, vol. 5 (1), pp. 26–35.
20. A. Zangiabadi and M. Kazeminezhad: *Comp. Mater. Sci.*, 2012, vol. 59, pp. 174–81.
21. S. Mehtonen, E. Palmiere, D. Misra, P. Karjalainen, and D. Porter: *ISIJ Int.*, 2014, vol. 54 (6), pp. 1406–15.
22. S. Mehtonen, P. Karjalainen, and D. Porter: *Mater. Sci. Forum*, 2013, vol. 762, pp. 705–10.
23. M.H. Farshidi, M. Kazeminezhad, and H. Miyamoto: *Mater. Sci. Eng. A*, 2014, vol. 615, pp. 139–47.
24. T. Sakai, A. Belyakov, R. Kaibyshev, H. Miura, and J.J. Jonas: *Prog. Mater. Sci.*, 2014, vol. 60, pp. 130–207.
25. J. Hamada, N. Ono, and H. Inoue: *ISIJ Int.*, 2011, vol. 51 (10), pp. 1740–48.
26. K.M. Lee, J. Park, S. Kim, S. Park, and M.Y. Huh: *Microsc. Microanal.*, 2013, vol. 19 (S5), pp. 17–20.
27. J.J. Jonas: *J. Mater. Process. Technol.*, 2001, vol. 117 (3), pp. 293–99.
28. M.R. Barnett and J.J. Jonas: *ISIJ Int.*, 1997, vol. 37 (7), pp. 706–14.
29. C.Z. Lu, Z. Fang, and J.Y. Li: *Mater. Charact.*, 2018, vol. 135, pp. 257–64.
30. J.T. Park and J.A. Szpunar: *Acta Mater.*, 2003, vol. 51 (11), pp. 3037–51.
31. R.P. Siqueira, H.R.Z. Sandim, T.R. Oliveira, and D. Raabe: *Mater. Sci. Eng. A*, 2011, vol. 528, pp. 3513–19.
32. Y. Hayakazawa and J.A. Szpunar: *Acta Mater.*, 1997, vol. 45 (11), pp. 4713–20.
33. S.K. Chang: *Mater. Sci. Eng. A*, 2007, vols. 452–453, pp. 93–98.
34. N. Chen, S. Zaefferer, L. Lahn, K. Gunther, and D. Raabe: *Acta Mater.*, 2003, vol. 51 (6), pp. 1755–65.